






## Synthesis and characterization of single phase ZnO nanostructures via solvothermal method: influence of alkaline source

Eric Kwabena Droepenu<sup>1,3,\*</sup> , Boon Siong Wee<sup>1,\*</sup> , Suk Fun Chin<sup>1</sup> , Kuan Ying Kok<sup>2</sup> , Ebenezer Aquisman Asare<sup>1,3</sup> 

<sup>1</sup>Resource Chemistry Program, Faculty of Resource Science and Technology, Universiti Malaysia Sarawak 94300, Kota Samarahan, Sarawak, Malaysia

<sup>2</sup>Malaysian Nuclear Agency, Bangi, Kajang, 43000 Selangor, Malaysia

<sup>3</sup>Graduate School of Nuclear and Allied Sciences, University of Ghana, AE1, Kwabenya-Accra, Ghana

\*corresponding author e-mail address: [kobladodzie01@yahoo.com](mailto:kobladodzie01@yahoo.com); [swboon@unimas.my](mailto:swboon@unimas.my) | Scopus ID [57194506096](https://orcid.org/0000-0001-9145-0609)

### ABSTRACT

Single phase ZnO nanostructures were synthesized by simple and low temperature solvothermal process from two different alkaline sources; Potassium hydroxide (KOH) and Sodium hydroxide (NaOH) with zinc acetate dihydrate ( $Zn(CH_3COO)_2 \cdot 2H_2O$ ) as precursor. This facile and rapid synthesis technique achieve high purity of Zinc oxide (ZnO) nanostructures on large scale negating the use of complex and high temperature routes. The synthesized particles were characterized by X-Ray Diffraction (XRD), Field Emission Scanning Electron Microscopy (FE-SEM), Transmission Electron Microscopy (TEM), Energy-dispersive X-ray spectroscopy (EDX), Fourier Transform Infrared (FT-IR) Spectroscopy, Ultraviolet Visible (UV-Vis) spectroscopy and Brunauer-Emmett-Teller (BET) analysis. ZnO synthesized using KOH and NaOH exhibit wurtzite hexagonal and flake-like nanostructures with average crystallite size of 11.0 nm and 14.9 nm respectively. Surface area of 59.50 m<sup>2</sup>/g and 31.43 m<sup>2</sup>/g were determined for KOH and NaOH sources respectively. The optical absorption spectra of the two samples showed absorption bands of 367.70 and 365.30 nm. The results showed the effect of alkaline sources on the surface morphology, structural and optical properties of ZnO.

**Keywords:** Nanostructures; Solvothermal synthesis; Alkaline source; Precursor; Microscopy; Spectroscopies.

### 1. INTRODUCTION

Technology today endeavor the use of crystalline particles in nanometric scale with uniform size and shape due to their numerous fascinating properties including catalytic, electrical and optical; which are desired in many promising applications. Among these, ZnO has attracted much attention because of its wide versatility in various fields such as pharmaceutical, electronics, cosmetics, optical and electrical devices, drug delivery and environmental remediation [1-6].

ZnO has many interesting properties including its wide band gap (3.37 eV), high bond strength, high thermal stability and large exciton binding energy (60 meV), which are required in electronics, optoelectronics and laser technologies [7-13]. Besides, ZnO also possesses good electrical, optical and antibacterial properties which are pre-requisite in the photoconductors, integrated sensors, electrodes and biomedicine industries [14-18].

Different routes have been used in synthesizing nanocrystalline ZnO powders as well as other nanostructures such as hydrothermal, spray pyrolysis, sol-gel, precipitation, microwave assisted, thermos-decomposition processes, micro-emulsion, electrodeposition, ultrasonic, microwave-assisted technique and chemical vapour deposition [19-27]. All these methods produce similar nanocrystalline structures based on different conditions. These conditions may arise from the precursor and alkaline

sources used, temperature variation, reaction time for nucleation of the nanoparticles as well as the calcination temperatures [28-30]. It should be noted that some of the methods employed in fabricating these nano-sized particles require complex processes and sophisticated equipment. Solvothermal technique, however, offers many great advantages over other techniques mentioned above. This technique requires simple setup, less expensive equipment, relatively low synthesis temperature to yield a large area of deposition. Also, it allows the microstructural control of the particles produced by altering experimental parameters such as temperature, reaction time, type of solvent, surfactant and precursor. Qualities of nanostructures in the manufacture of devices such as sensors, photo diodes, transistors are based on the shape, size and purity of the synthesized nanoparticles. These properties can also be achieved using simple experimental set-ups with minimum reaction conditions not necessarily using highly complex equipment under very high reaction conditions. It is against this backdrop that the current study employed two alkaline sources (KOH and NaOH) in synthesizing ZnO NPs with Zinc acetate dihydrate precursor in a solvothermal method at relatively lower reaction conditions to achieve high quality ZnO nanostructures. The quality of the ZnO produced was investigated using a series of physiochemical characterization tools.

### 2. MATERIALS AND METHODS

#### 2.1. Materials.

Zinc acetate dihydrate [ $Zn(CH_3COO)_2 \cdot 2H_2O$ ], Potassium hydroxide (KOH), Sodium hydroxide (NaOH), 95% Absolute

Ethanol ( $C_2H_5OH$ ). All chemicals were of analytical reagent grade from Sigma-Aldrich without further purification.

## 2.2. Synthesis of Zinc oxide (ZnO) Nanoparticles (NPs).

Synthesis of ZnO NPs was based on the solvothermal technique reported by [31] with slight modification. A weighed mass of  $1.83 \pm 0.1$  g (0.01 mol) of  $[\text{Zn}(\text{CH}_3\text{COO})_2 \cdot 2\text{H}_2\text{O}]$ , [Sigma-Aldrich, India] was dissolved in 100 mL of absolute ethanol in a 250 mL Schott bottle and heated to a temperature of  $60^\circ\text{C}$  with constant stirring using electrical stirring hotplate (Favorit). Subsequently,  $5.60 \pm 0.1$  g (0.01 mol) of KOH (VWR Amresco, US) was also weighed and dissolved in 100 mL of absolute ethanol in 250 mL Schott bottle under the same condition as the Zinc acetate. After complete dissolution, the alkaline solution (KOH) was slowly drained dropwise from a burette into the  $\text{Zn}(\text{CH}_3\text{COO})_2 \cdot 2\text{H}_2\text{O}$  solution, maintaining the temperature at  $60^\circ\text{C}$  with vigorous stirring for 60 minutes until white precipitate was formed. The mixture was allowed to cool at room temperature for 180 minutes before centrifuging with FLETA 5 Multi-Purpose Centrifuge at 4000 rpm for 30 minutes. The precipitate was filtered using  $0.45 \mu\text{m}$  Whatman filter membrane, washed twice with acetone and then with deionized water, dried at room temperature and finally ground in a powdery form for characterization. The same process was repeated for the NaOH (VWR Amresco, US) where  $4.0 \pm 0.1$  g (0.01 mol) was weighed into 100 mL of 95% absolute ethanol under the same reaction conditions.

## 2.3. Characterization of synthesized ZnO.

The synthesized samples were characterized using X-ray Diffraction, XRD, (Xpert Pro MPD PW3040/60) for their crystal structure and crystallite size. Diffraction patterns from the XRD analysis in Figure 1 (a & b) were obtained using X-ray diffractometer with  $\text{Cu-K}\alpha$  radiation of 40 kV and 30 mA with step size of  $0.017^\circ$ . The morphology of ZnO NPs was determined using Field Emission Scanning Electron Microscopy (Carl Zeiss GeminiSEM 500) with acceleration voltage of 10.0 kV, the working distance of 11.6 mm and a chamber pressure of 40 Pa. Sample preparation for FE-SEM, TEM, EDX, FT-IR and UV-vis

analysis was carried out using the method outlined by [32]. The powdered solid ZnO NPs were coated on a silicon wafer with the help of a carbon tape. Before the FE-SEM imaging, the dry powders were mounted on a stub followed by coating with Platinum (Pt) for 1 minute using a sputter coater. TEM analysis was done using TEM (JEOL 1230, Japan). Powdered ZnO NPs were first diluted with absolute ethanol (95%) and sonicated with ultrasonic cleaner (Elma, Germany) for 30 minutes. A  $4 \mu\text{l}$  of the solution sample was loaded onto a Foamvar film Copper grid (FF300-Cu) before being observed under TEM. The purity of the ZnO NPs was determined with EDX (JEOL 6390LA, Japan). The ZnO NPs were diluted with 95% Absolute ethanol and sonicated with ultrasonic cleaner (Elma, Germany) for 30 minutes. A  $4 \mu\text{l}$  of ZnO NPs sample was loaded onto an aluminium plate before being analyzed.

FT-IR (Thermo Scientific Nicolet iS10, US) and UV-Vis (UV-1800 SHIMADZU UV Spectrophotometer) was used to determine the surface functional groups and the optical property of the sample. The FT-IR sample preparation involved mixing the powdered ZnO with Potassium bromide (KBr) in the ratio of 1: 19 [33]. The sample was then placed in the metal hole, pressed until the sample compressed inside the hole, and analyzed using FT-IR. In the case of UV-Vis, the spectral range of  $4000\text{--}400 \text{ cm}^{-1}$  with resolution of  $4 \text{ cm}^{-1}$  was used. The optical property of the samples was determined by measuring their maximum absorbance using UV-vis spectrophotometry. The ZnO-NPs were dispersed in ethanol and sonicated for 10 minutes before it was used for the measurement.

In addition, Brunauer-Emmett-Teller (BET) (Quantachrome, US Autosorb iQ, version 2.01) was used for the surface area determination. Approximately, 0.3 g of ZnO NPs powder was degassed at  $175^\circ\text{C}$  for 2 hours [34] in a flowing  $\text{N}_2$  gas. The  $\text{N}_2$  absorption-desorption isotherms of the samples were then be measured.

## 3. RESULTS

### 3.1. Structural Properties.

#### 3.1.1. XRD Results.

The XRD pattern of the ZnO prepared by the solvothermal process at  $60^\circ\text{C}$  for 180 minutes from KOH and NaOH alkaline source is shown in Figure 1 (a & b). All detectable peaks can be indexed to ZnO wurtzite structure with ICSD Number (ICSD: 98-000-9346) and PDF Number (Experimental and calculated powder diffraction data) of 36-1451 and 01-074-0534 respectively. The patterns are broadened due to the nanosize of the ZnO crystals [35,31,36]. Based on the XRD diffraction patterns, all synthesized ZnO NPs were identified as being 100 % pure ZnO. The average crystallite size of the samples was calculated using Scherer's formula [37].

$$D = \frac{K\lambda}{\beta \cos\theta} \quad (1)$$

where;

K = shape factor = 0.89

$$\beta = \sqrt{\beta_{FWHM}^2 - \beta_0^2} \quad (2)$$

the peak broadening after removing the instrumental broadening.

$\beta_{FWHM}$  is the full width half maximum of the diffraction peak and  $\beta_0$  is the correction factor for instrumental broadening ( $0.07^\circ 2\theta$ ).

The average crystallite size of ZnO prepared using KOH determined from the Panalytical X'Pert Pro MPD, diffraction peak was found to be  $11.0 \pm 1.3$  nm whereas the sample synthesized using NaOH was  $14.9 \pm 1.2$  nm. When these results were compared to a study by Ramachandra et al., the crystallite size determined in their study was 43 nm and 45 nm using hydrothermal method at a reaction temperature of  $150^\circ\text{C}$  and calcination temperature of  $600^\circ\text{C}$  [38]. This is evident that, despite the simplicity and moderate conditions employed in this study, smaller crystallite sizes could be produced. According to [39], a crystallite size of 21.59 nm and 36.89 nm can be obtained for ZnO from KOH and NaOH, respectively in a sol-gel method. Their reaction time and drying temperature were maintained at 2 hours and  $70^\circ\text{C}$ . In another study by [24], an average crystallite size of 33 nm was recorded in a solvothermal method using Zinc acetate and Triethanolamine (TEA) media. In their study, the TEA/ $\text{Zn}^{2+}$  solution was autoclaved at  $150^\circ\text{C}$  for 18 hours.

#### 3.1.2. FE-SEM and TEM Results.

The FE-SEM and TEM images of ZnO nanoparticles prepared from KOH and NaOH alkaline sources are shown in Figure 2 (a & b) and Figure 2 (c & d) respectively. The FE-SEM

and TEM images of the two samples show agglomeration/aggregation of the particles. FE-SEM and TEM images of ZnO NPs synthesized from KOH source (Figure 2 a & c) confirm the formation of homogeneous hexagonal wurtzite structures.

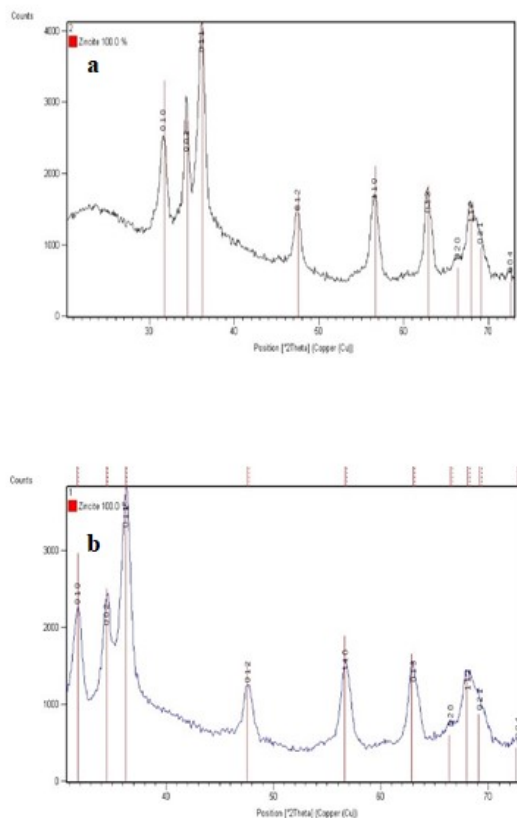


**Figure 1.** XRD diffractogram of ZnO nanoparticles synthesized using (a) KOH and (b) NaOH.

The sample synthesized using KOH displayed morphology similar to the nanostructures obtained by [24], when zinc acetate and Triethanolamine (TEA) were used in a solvothermal method autoclaved at a temperature of 150 °C for 18 hours. Samples shown in Figure 2a have a high surface area due to their small particle size, rendering them appropriate for catalytic applications [40].

When NaOH was used under the same experimental conditions, the morphology changed to flake-like nanostructures as depicted in Figure 2 (b). Its corresponding TEM image, Figure 2 (d) also shows flake-like nanostructures. For nanocrystalline ZnO powder synthesized by sol-gel method, flake-like nanostructures were fabricated at a lower concentration as Polyvinylpyrrolidone (PVP) was used as a capping agent when  $\text{Zn}(\text{ZnCH}_3\text{COO})_2 \cdot 2\text{H}_2\text{O}$  was reacted with NaOH and calcined at a temperature of 600 °C [41]. In other study by Gopal and Kamila, ZnO flake-like nanostructures were obtained from a reaction of zinc nitrate and NaOH using precipitation technique at a calcination temperature of between 400-600 °C [42]. Apart from Gopal and Kamila, other studies that fabricated flake-like nanostructures using different synthesis techniques include [43-46]. In all these studies, complicated methods, expensive equipment with very critical reaction conditions were used as compared to this study. Table 1 below gives a summary of the conditions and the particle size synthesized by the different studies.

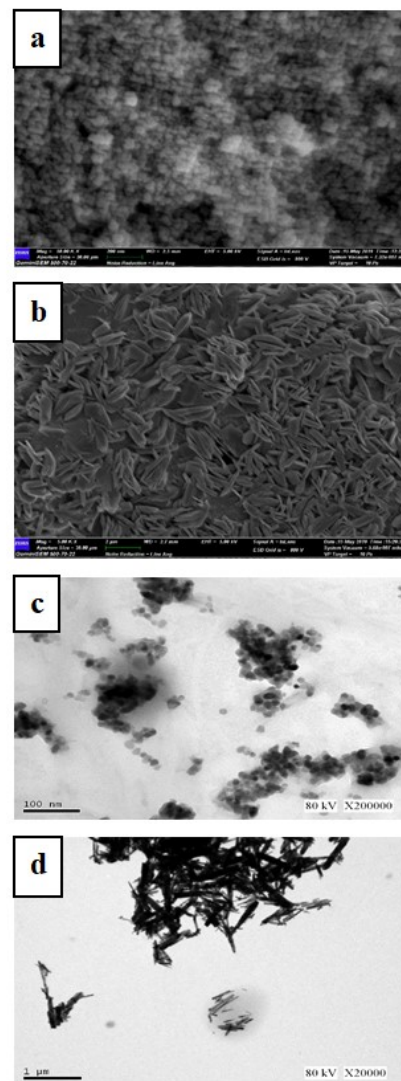


**Figure 2.** FE-SEM images of synthesized ZnO NPs with (a) KOH and (b) NaOH, alkaline source and TEM images of synthesized ZnO NPs with (c) KOH and (d) NaOH alkaline source.

### 3.1.3. FT-IR Results.

The FT-IR spectra of ZnO NPs synthesized from KOH and NaOH are shown in Figure 3. The characteristic band of wurtzite ZnO in the two samples occurred at peaks of 420  $\text{cm}^{-1}$  and 422  $\text{cm}^{-1}$  respectively. This agrees with [51-53,33], who estimated the range to be between 400-500  $\text{cm}^{-1}$ .

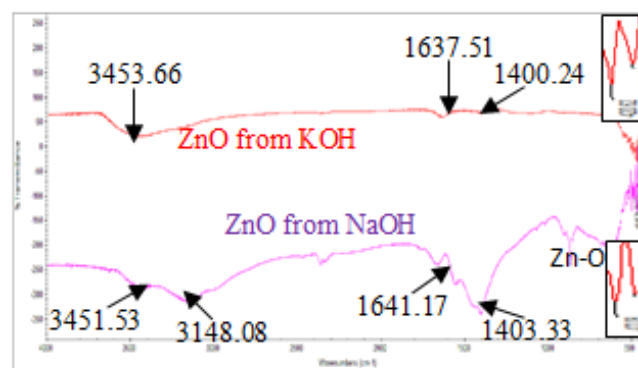


**Figure 3.** FT-IR spectra of ZnO NPs synthesized from KOH and NaOH alkaline source.

Both samples show broad absorption bands in the peak range of 3500-3700 and 1400-1600  $\text{cm}^{-1}$  (in the case of ZnO from NaOH) corresponding to O-H stretching and bending of hydroxyl

group [54-56]. But in the case of ZnO synthesized from KOH, peaks within the 1400-1600  $\text{cm}^{-1}$  range diminishes. It can also be observed that asymmetric and symmetric C=O stretching of zinc acetate is intense in ZnO synthesized from NaOH than that of KOH at peak range of 1640 and 1500  $\text{cm}^{-1}$  [41]. This might be the effect of difference in pH which results in low rate of transformation thereby introducing some carboxylate (-COO-) functional group [57]. The -C-H bending in alkane is much more intense in the ZnO synthesized from NaOH than the one from KOH which occurs at 1400  $\text{cm}^{-1}$ .

3.1.4. UV-Vis Results

The UV-Vis absorption spectra of ZnO NPs synthesized using NaOH and KOH respectively are illustrated in Figure 4 (a & b). The absorption spectra of the synthesized samples were acquired using UV-Vis spectrophotometer in the wavelength region of 300-400 nm. The spectrum reveals a strong characteristic absorption band of ZnO at wavelength of 367.70 nm and 365.30 nm for the KOH and NaOH alkaline source respectively. The absorption depends on factors such as band gap, oxygen deficiency, size and structure of the nanoparticles, surface roughness and impurity centers [58]. The good absorption characteristics of the ZnO-NPs in the UV region proves its suitability in applications such as sunscreen protectors or antiseptic ointments [59-60].

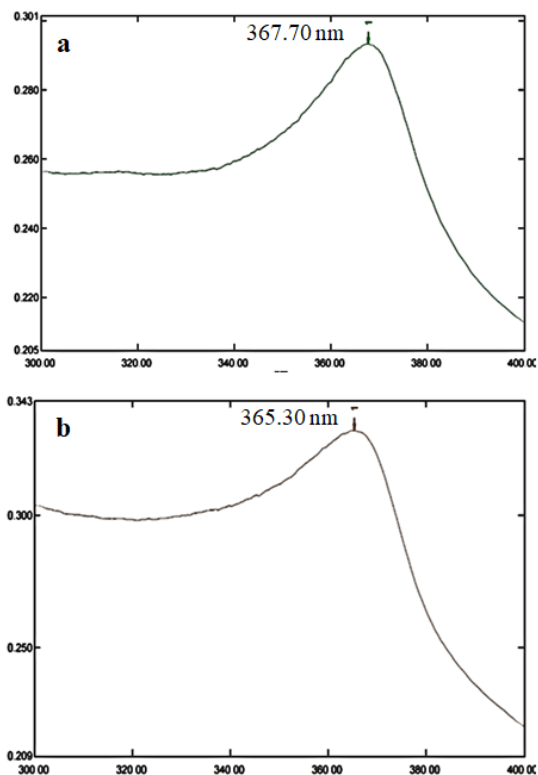


Figure 4. Optical absorption Spectra of ZnO NPs synthesized using (a) KOH and (b) NaOH.

3.1.5. EDX Results.

EDX spectroscopy was used to provide elemental analysis of the particles and is displayed in the spectra in Figure 5 (a & b).

The spectra show the presence of two main elements, namely Zn and O in the proportion of 75.2%: 24.8% and 73.9%:26.1% for samples A and B respectively. When these data were compared to the theoretical value of Zn and O (80.3:19.7) by [61], it can be concluded that the synthesized ZnO nanostructures

were of high purity. Similar findings were also reported in previous studies by [62,49,31].

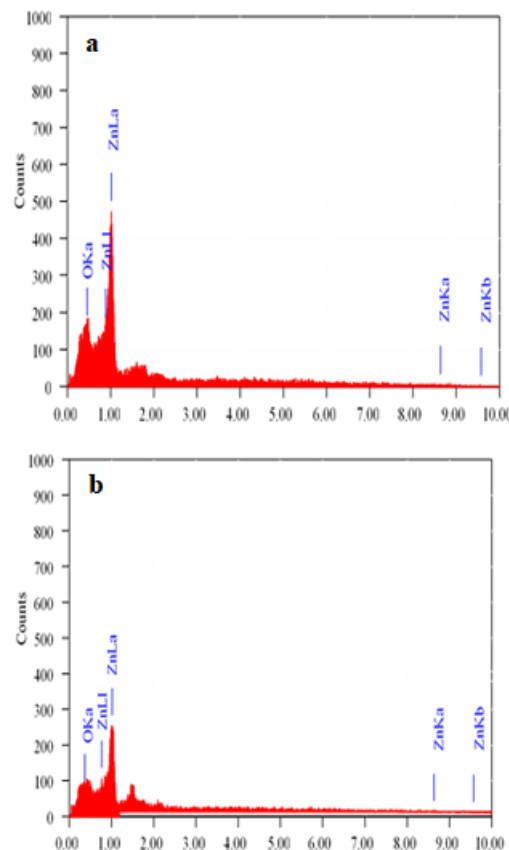


Figure 5. EDX spectra of ZnO NPs synthesized using (a) KOH and (b) NaOH.

3.1.6. BET Results

Figure 6 (A and B) shows the BET analysis isotherms of ZnO NPs synthesized using KOH and NaOH.

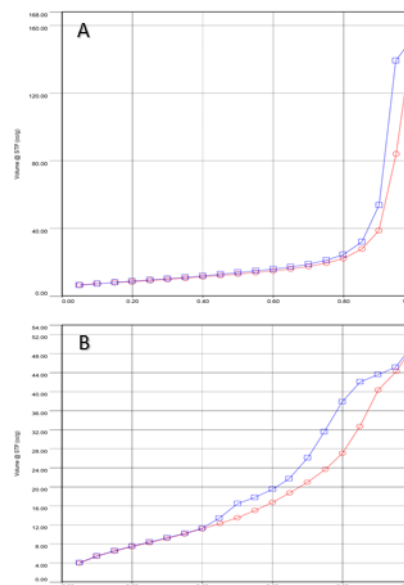


Figure 6. Nitrogen (N<sub>2</sub>) adsorption- desorption isotherms of ZnO NPs synthesized using (A) KOH and (B) NaOH alkaline sources.

The specific surface area was also determined to be 59.50  $\text{m}^2/\text{g}$  and 31.43  $\text{m}^2/\text{g}$  for the zinc oxide NPs synthesized from KOH and NaOH respectively. This suggests that sample A shows a large surface area as compared to sample B. Furthermore, the

average particle size calculated from BET data for sample A due to its spherical shape was 16.5 nm based on the equation;

$$PS_{BET} = \frac{6000}{SA_{BET} \times \rho} \quad (3)$$

where;  $PS_{BET}$  is the average particle size determined by BET,  $\rho$  is the theoretical density of the sample which was  $6.11 \text{ g cm}^{-3}$ , and  $SA_{BET}$  is the obtained surface area [34,63].

Table 1. Characteristics of ZnO nanostructures synthesized by different studies.

Precursor Zinc and Alkali salt	Synthesis condition	Properties	Reference
$\text{Zn}(\text{CH}_3\text{COO})_2 \cdot 2\text{H}_2\text{O} + \text{KOH}$	Reaction temp: 60 °C Reaction time: 3 h Drying temp: room temp.	Ave. crystallite size: 11.0	Current study
$\text{Zn}(\text{CH}_3\text{COO})_2 \cdot 2\text{H}_2\text{O} + \text{NaOH}$	Same conditions as above.	Ave. crystallite size: 14.9	
$\text{Zn}(\text{CH}_3\text{COO})_2 + \text{NaOH}$	Reaction temp: 25 °C Drying: 100 °C 4 h Calcined: 400 °C 2 h Reaction time: 7 h Synthesis time: 8 h	Particle size: 97-174 nm Ave. crystallite size: 23.04 nm	[42]
$\text{Zn}(\text{NO}_3)_2 + \text{NaOH}$	Synthesis condition same as the above	Particle size: 52-93 nm Ave. crystallite size: 19 nm	
$\text{Zn}(\text{SO}_4)_2 + \text{NaOH}$	Synthesis condition same as the above	Particle size: 49-179 nm Ave. crystallite size: 37 nm	
$\text{Zn}(\text{CH}_3\text{COO})_2 + (\text{TEA}) + \text{NaOH}$	Reaction temp: 60 °C Drying: 60 °C overnight Calcined: 150 °C 18 h	Particle size: $48 \pm 7$ nm Ave. crystallite size: $23 \pm 2$ nm	[22]
$\text{Zn}(\text{NO}_3)_2 \cdot 6\text{H}_2\text{O} + \text{NaOH}$	Reaction temp: 150 °C Reaction time: 7 h Calcined: 600 °C 1 h	Pore diameter size: 9-12 nm Ave. crystallite size: 45 & 43 nm	[38]
$\text{Zn}(\text{CH}_3\text{COO})_2 \cdot 2\text{H}_2\text{O} + \text{Polyvinylpyrrolidone (PVP)} + \text{NaOH}$	Reaction time: 1 h Drying: 60 °C Calcined: 600 °C 1 h	Ave. crystallite size: 45, 48, 49, & 56 nm for different conc. of PVP Particle size: 150 nm	[41]
$\text{Zn}(\text{CH}_3\text{COO})_2 \cdot 2\text{H}_2\text{O} + \text{N}_2\text{H}_4$	Irradiation: 15 min 510W 10 min 680 W Drying: 100 °C 2 h		[43]
$\text{Zn}(\text{NO}_3)_2 \cdot 6\text{H}_2\text{O} + \text{NaOH} + \text{NH}_3$	Irradiation: 15 min 150 W Drying: 100 °C 2 h Calcination: 600 °C 3 h	Needle shaped structure Flower shaped structures Particle diameter: 50-150 nm	
$\text{Zn}(\text{CH}_3\text{COO})_2 \cdot 2\text{H}_2\text{O} + \text{CTAB} + \text{NaOH}$	Reaction temp: 25, 35, 55 & 75 °C	Particle size: 23.7-88.8 nm Crystallite size: 23.7, 82.5, 69.6 & 88.8 nm	[45]
$\text{Zn}(\text{CH}_3\text{COO})_2 \cdot 2\text{H}_2\text{O} + \text{NaOH}$	Reaction temp: 90 °C Reaction time: 2 h	Crystallite size: 75 & 54 nm	[46]
$\text{Zn}(\text{CH}_3\text{COO})_2 \cdot 2\text{H}_2\text{O} + (\text{CTAB}) + \text{NaOH}$	Reaction time: 50 min Reaction temp: 25 °C Drying: 60 °C 2h	Particle diameter: 10-30 nm Particle length: 150-250 nm	[47]
$\text{Zn}(\text{CH}_3\text{COO})_2 \cdot 2\text{H}_2\text{O} + \text{KOH}$	Reaction time: 3 h Reaction temp: 60 °C Drying: room temp.	Particle size: $7.4 \pm 1.2$ nm Crystallite size: 10.08 nm	[31]
$\text{Zn}(\text{CH}_3\text{COO})_2 \cdot 2\text{H}_2\text{O} + \text{NaOH}$ Conc. ratio (1:1, 1:2, 1:4, 1:8)	Reaction time: 1-3 h Reaction temp: 120 °C Drying: 100 °C	Crystallite size: 300 nm to 10 $\mu\text{m}$	[48]
$\text{Zn}(\text{CH}_3\text{COO})_2 \cdot 2\text{H}_2\text{O} + \text{NaOH}$	Reaction temp: room temp Drying temp: 100 °C 5 h Calcination: 250 °C 3 h	Crystallite size: 20-36 nm Particle size: 18-36 nm	[49]
$\text{Zn}(\text{NO}_3)_2 + \text{NaOH}$	Reaction time: 2 h + 24 h Drying: 70 °C for several hours	Crystallite size: 36.89 and 21.59 nm Particle size: 17-25 nm	[39]
$\text{Zn}(\text{NO}_3)_2 + \text{KOH}$		Crystallite size: 21.59 nm Particle size: 30-50 nm	
$\text{Zn}(\text{CH}_3\text{COO})_2 \cdot 2\text{H}_2\text{O} + \text{NaOH}$	Reaction Temp: 25 °C Reaction time: 7 h Drying: 100 °C for 4 H Calcination: 400 °C for 2 h Synthesis time: 8 h	Crystallite/Particle size: 23.04 nm/97-174 nm Crystallite/Particle size: 19.00 nm/52-93 nm Crystallite/Particle size: 37.00 nm/49-179 nm	[28]
$\text{Zn}(\text{CH}_3\text{COO})_2 \cdot 2\text{H}_2\text{O} + \text{C}_2\text{H}_4(\text{OH})_2$	Reaction temp: 70 °C Microwave radiation: 600 W, 2.45 GHz Reaction time: 25 min 220 °C Drying: freeze drying	Particle size: 25-50 nm Crystallite size: 23-48 nm	[50]



#### 4. CONCLUSIONS

Single phase ZnO nanostructures were successfully synthesized by a simple and low temperature solvothermal process from two different alkaline sources (KOH and NaOH) with zinc acetate dehydrate ( $\text{Zn}(\text{CH}_3\text{COO})_2 \cdot 2\text{H}_2\text{O}$ ) as the precursor. The synthesis technique achieved a high purity ZnO nanostructures with wurtzite hexagonal and flake-like nanostructures of average crystallite size of 11.0 nm and 14.9 nm for the two alkaline source respectively. The average surface area of 59.50  $\text{m}^2/\text{g}$  and 31.43

$\text{m}^2/\text{g}$  was determined for ZnO NPs obtained from KOH and NaOH sources respectively. The optical absorption spectra of the two samples showed absorption bands of 367.70 and 365.30 nm as an indication for a pure ZnO NPs. EDX has also proven the purity of synthesized samples to contain high Zn and O element composition. The study showed that the type of alkaline source used has a significant effect the surface morphology, structural and optical properties of ZnO NPs.

#### 5. REFERENCES

- Jiang, J.; Pi, J.; Cai, J. The advancing of zinc oxide nanoparticles for biomedical applications. *Bioinorganic Chemistry and Applications* **2018**, 2018, 1-18, <https://doi.org/10.1155/2018/1062562>.
- Chaudhary, S.; Umar, A.; Bhasin, K.K.; Baskoutas, S. Chemical Sensing Applications of ZnO Nanomaterials. *Materials* **2018**, 11(287), 1-38, <https://doi.org/10.3390/ma11020287>.
- Jafari, M.; Soltani, M.; Naahidi, S.; Karunaratne, N.; Chen, P. Nonviral approach for targeted nucleic acid delivery. *Current Medicinal Chemistry* **2012**, 19, 197-208, <https://doi.org/10.2174/092986712803414141>.
- Naahidi, S.; Jafari, M.; Edalat, F.; Raymond, K.; Khademhosseini, A.; Chen, P. Biocompatibility of engineered nanoparticles for drug delivery. *Journal of Controlled Release* **2013**, 166, 182-194, <https://doi.org/10.1016/j.jconrel.2012.12.013>.
- Sarmah, K.; Pratihari, S. Synthesis, characterization and photocatalytic application of iron oxalate capped Fe, Fe-Cu, Fe-Co, and Fe-Mn oxide nanomaterial. *ACS Sustainable Chemistry & Engineering* **2017**, 5, 310-324, <https://doi.org/10.1021/acssuschemeng.6b01673>.
- Das, P.; Sarmah, K.; Hussain, N.; Pratihari, S.; Das, S.; Bhattacharyya, P.; Patil, S.A.; Kim, H.S.; Iqbal, M.; Khazie, A.; Bhattacharyya, S.S. Novel synthesis of an iron oxalate capped iron oxide nanomaterial; a unique soil conditioner and slow release eco-friendly source of iron sustenance in plants. *RSC Advances* **2016**, 6, 103012-25, <https://doi.org/10.1039/C6RA18840K>.
- Ashrafi, A.; Jagadish, C. Review of zincblende ZnO: stability of metastable ZnO phases. *Journal of Applied Physics* **2007**, 10, <https://doi.org/10.1063/1.2787957>.
- Bacaksiz, E.; Parlak, M.; Tomakin, M.; Ozcelik, A.; Karakiz, M.; Altunbas, M. The effects of zinc nitrate, zinc acetate and zinc chloride precursors on investigation of structural and optical properties of ZnO thin films. *Journal of Alloys & Compounds* **2008**, 466, 447-450, <https://doi.org/10.1016/j.jallcom.2007.11.061>.
- Ozgur, U.; Hofstetter, D.; Morkoc, H. ZnO devices and applications: a review of current status and future prospects. *Proceedings of the Institute of Electrical and Electronic Engineers* **2010**, 98, 1255-1268, <https://doi.org/10.1109/JPROC.2010.2044550>.
- Djurisic, A.B.; Ng, A.M.C.; Chen, X.Y. ZnO nanostructures for optoelectronics: material properties and device applications. *Progress in Quantum Electronics* **2010**, 34, 191-259, <https://doi.org/10.1016/j.pquantelec.2010.04.001>.
- Willander, M.; Zhao, Q.X.; Hu, Q.H.; Klason, P.; Kuzmin, V.; Al-Hilli, S.M.; Nur, O.; Lozovik, Y.E. Fundamentals and properties of zinc oxide nanostructures: optical and sensing applications. *Superlattices and Microstructures* **2008**, 43, 352-361, <https://doi.org/10.1016/j.spmi.2007.12.021>.
- Bao, D.; Gu, H.; Kuang, A. Sol-gel-derived c-axis oriented ZnO thin films. *Thin Solid Films* **1998**, 312, 37-39, [https://doi.org/10.1016/S0040-6090\(97\)00302-7](https://doi.org/10.1016/S0040-6090(97)00302-7).
- Majumder, S.B.; Jain, M.; Dobal, P.S.; Katiyar, R.S. Investigations on solution derived aluminium doped zinc oxide thin films. *Material Science and Engineering: B* **2003**, 103, 16-25, [https://doi.org/10.1016/S0921-5107\(03\)00128-4](https://doi.org/10.1016/S0921-5107(03)00128-4).
- Sirelkhatim, A.; Mahmud, S.; Seeni, A.; Mohamad, N.H. Review on zinc oxide nanoparticles: antibacterial activity and toxicity mechanism. *Nano-Micro Letters* **2015**, 7, 219-242, <https://doi.org/10.1007/s40820-015-0040-x>.
- Zhang, Y.; Nayak, T.R.; Hong, H.; Cai, W. Biomedical applications of zinc oxide nanomaterials. *Current Molecular Medicine* **2013**, 13, 1633-1645, <https://doi.org/10.2174/156652401366613111130058>.
- Lee, K.M.; Lai, C.W.; Ngai, K.S.; Juan, J.C. Recent developments of zinc oxide based photocatalyst in water treatment technology: a review. *Water Research*. **88**, **2016**, 428-448, <https://doi.org/10.1016/j.watres.2015.09.045>.
- Pimentel, A.; Samouco, A.; Nunes, D.; Araújo, A.; Martins, R.; Fortunato, E. Ultra-Fast Microwave Synthesis of ZnO Nanorods on Cellulose Substrates for UV Sensor Applications. *Materials* **2018**, 10(1308), 1-18, <https://doi.org/10.3390/ma10111308>.
- Xu, J.; Pan, Q.; Shun, Q.; Tian, Z. Grain size control and gas sensing properties of ZnO gas sensor. *Sensors and Actuators B: Chemical* **2000**, 66, 277-279, [https://doi.org/10.1016/S0925-4005\(00\)00381-6](https://doi.org/10.1016/S0925-4005(00)00381-6).
- Pal, S.K.; Thapa, K.B. Synthesis and characterization of ZnO nano-particles for solar cell application by the cost effective co-precipitation method without any surfactants. *AIP Conference Proceedings* **2019**, <https://doi.org/10.1063/1.5122336>.
- Ananthakumar, S.; Kumar, J.R.; Babu, S.M. Evolution of non-phosphine solvents in colloidal synthesis of I-III-VI 2 and I 2 -II-IV-VI 4 group semiconductor nanomaterials – Current status. *Material Science in Semiconductor Process* **2017**, 67, 152-174, <https://doi.org/10.1016/j.mssp.2017.05.005>.
- Gromova, M.; Lefrancois, A.; Vaure, L.; Agnese, F.; Aldakov, D.; Maurice, A.; Djurado, D.; Lebrun, C.; de Geyer, A.; Schulli, T.U.; Pouget, S.; Reiss, P. Growth Mechanism and Surface State of CuInS<sub>2</sub> Nanocrystals Synthesized with Dodecanethiol. *Journal of the American Chemical Society* **2017**, 139, 15748-15759, <https://doi.org/10.1021/jacs.7b07401>.
- Zak, A.K.; Abrishami, M.E.; Majid, W.H.; Abd. Yousefi, R.; Hosseini, S.M. Effects of annealing temperature on some structural and optical properties of ZnO nanoparticles prepared by a modified sol-gel combustion method. *Ceramics International* **2011**, 37:393-398, <https://doi.org/10.1016/j.ceramint.2010.08.017>.
- Wang, Y.; Zhang, C.; Bi, S.; Luo, G. Preparation of ZnO nanoparticles using the direct precipitation method in a membrane dispersion microstructured reactor. *Powder Technology* **2010**, 202, 130-136, <https://doi.org/10.1016/j.powtec.2010.04.027>.

24. Sangkhaoprom, N.; Supaphol, P.; Pavarajarn, V. Fibrous zinc oxide prepared by combined electrospinning and solvothermal techniques. *Ceramics International* **2010**, *36*, 357–360, <https://doi.org/10.1016/j.ceramint.2009.09.014>.
25. Li, S.; Tang, X.; Zang, Z.; Yao, Y.; Yao, Z.; Zhong, H.; Chen, B. I-III-VI chalcogenide semiconductor nanocrystals: Synthesis, properties, and applications. *Chinese Journal of Catalysis* **2018**, *39*, 590–605, [https://doi.org/10.1016/S1872-2067\(18\)63052-9](https://doi.org/10.1016/S1872-2067(18)63052-9).
26. Kwoka, M.; Lyson-Sypien, B.; Kulis, A.; Maslyk, M.; Borysiewicz, M.A.; Kaminska, E.; Szuber, J. Surface Properties of Nanostructured, Porous ZnO Thin Films Prepared by Direct Current Reactive Magnetron Sputtering. *Materials* **2018**, *11*(31), 1–11, <https://doi.org/10.3390/ma11010131>.
27. Mishra, P.; Yadav, R.S.; Pandey, A.C. Growth mechanism and photoluminescence property of flower-like ZnO nanostructures synthesized by starch-assisted sonochemical method. *Ultrasonics Sonochemistry* **2010**, *17*, 560–565, <https://doi.org/10.1016/j.ultsonch.2009.10.017>.
28. Gopal, V.R.V.; Kamila, S. Effect of temperature on the morphology of ZnO nanoparticles: a comparative study. *Applied Nanoscience* **2017**, *7*, 75–82, <https://doi.org/10.1007/s13204-017-0553-3>.
29. Etcheverry, L.P.; Flores, W.H.; da Silva, D.L.; Moreira, E.C. Annealing effects on the structural and optical properties of ZnO nanostructures. *Materials Research* **2018**, *21*(2), <https://doi.org/10.1590/1980-5373-mr-2017-0936>.
30. Yang, J.; Li, J.; Zhu, Y.; Xu, X.; Xiao, X.; Deng, B.; Qin, K.; Bi, Z.; Chen, S.; Xu, G. Low-Temperature Synthesis of Highly Efficient, Deep-Red Zn-Cu-In-Se/ZnSe Fluorescence Quantum Dots. *NANO: Brief Reports and Reviews* **2019**, *14*, 10, <https://doi.org/10.1142/S179329201950070X>.
31. Nuraqeelah, M.S.; Wee, B.S.; Chin, S.F.; Kok, K.Y. Synthesis and characterization of zinc oxide nanoparticles with small particle size distribution. *Acta Chimica Slovenica* **2018**, *65*, 578–585, <http://dx.doi.org/10.17344/acs.2018.4213>.
32. Droepenu, E.K.; Asare, E.A. Morphology of green synthesized ZnO nanoparticles using low temperature hydrothermal technique from aqueous *Carica papaya* extract. *Nanoscience and Nanotechnology* **2019**, *9*, 29–36, <https://doi.org/10.5923/j.nn.20190901.03>.
33. Yang, K.; Lin, D.; Xing, B. Interactions of humic acid with nanosized inorganic oxides. *Langmuir* **2009**, *25*, 3571–3576, <https://doi.org/10.1021/la803701b>.
34. Zhou, M.; Wei, Z.; Qiao, H.; Zhu, L.; Yang, H.; Xia, T. Particle size and pore structure characterization of silver nanoparticles prepared by confined arc plasma. *Journal of Nanomaterials* **2009**, *2009*, 5, <http://dx.doi.org/10.1155/2009/968058>.
35. Bai, X.; Li, L.; Liu, H.; Tan, L.; Liu, T.; Meng, X. Solvothermal synthesis of ZnO nanoparticles and anti-infection application in vivo. *ACS Applied Materials & Interface* **2015**, *7*, 1308–1317, <https://doi.org/10.1021/am507532p>.
36. Wang, Y.X.; Sun, J.; Yu, X. A CTAB hydrothermal and solvothermal synthesis of ZnO nanopowders. *Ceramics International* **2011**, *37*, 3431–3436, <https://doi.org/10.1016/j.ceramint.2011.04.134>.
37. Cullity, B.D. *Elements of X-ray Diffractions*. Addison-Wesley Publishing, 1957.
38. Ramachandra, A.R.; Mallika, A.N.; Sowri, K.B.; Venugopal, K.R. Hydrothermal synthesis and characterization of ZnO nano crystals. *Strain ( $\epsilon$ )* **2015**, *10*, 10–4, <http://www.isaet.org/images/extraimages/P315056.pdf>
39. Vanaja, A.; Srinivasa, R.K. Effect of solvents on particle structure, morphology and optical properties of zinc oxide nanoparticles. *International Journal in Advances in Material Science & Engineering* **2015**, *4*, 1–8, <https://doi.org/10.14810/ijamse.2015.4201>.
40. Jang, E.S.; Won, J.H.; Hwang, S.J.; Choy, J.H. Fine tuning of the face orientation of ZnO crystals to optimize their photocatalytic activity. *Advanced Materials* **2006**, *18*, 3309–3312, <https://doi.org/10.1002/adma.200601455>.
41. Suwanboon, S. Structural and optical properties of nanocrystalline ZnO powder from sol-gel method. *ScienceAsia* **2008**, *34*: 031–034. <https://doi.org/10.2306/scienceasia1513-1874.2008.34.031>.
42. Gopal, V.V.R.; Kamila, S. Effect of temperature on the morphology of ZnO nanoparticles: a comparative study. *Applied Nanoscience* **2017**, *7*, 75–82, <https://doi.org/10.1007/s13204-017-0553-3>.
43. Hasanpoor, M.; Aliofkhaezrai, M.; Delavari, H. Microwave-assisted synthesis of zinc oxide nanoparticles. *Procedia Material Science* **2015**, *11*, 320–325, <https://doi.org/10.1016/j.mspro.2015.11.101>.
44. Kataria, N.; Garg, V.K.; Jain, M.; Kadirvelu, K. Preparation, characterization and potential use of flower shaped zinc oxide nanoparticles (ZON) for the adsorption of Victoria Blue B dye from aqueous solution. *Advanced Powder Technology* **2016**, *27*, 1180–1188, <https://doi.org/10.1016/j.apt.2016.04.001>.
45. Khan, M.F.; Hameedullah, M.; Ansari, A.H.; Ahmad, E.; Lohani, M.B.; Khan, R.H.; Alam, M.M.; Khan, W.; Husain, F.M.; Ahmed, I. Flower-shaped ZnO nanoparticles synthesized by a novel approach at near-room temperatures with antibacterial and antifungal properties. *International Journal of Nanomedicine* **2014**, *9*, 853–864, <https://dx.doi.org/10.2147%2FIJN.S47351>.
46. Osman, D.A.M.; Mustafa, M.A. Synthesis and characterization of zinc oxide nanoparticles using zinc acetate dihydrate and sodium hydroxide. *Journal of Nanoscience and Nanoengineering* **2015**, *1*, 248–251, <http://www.aiscience.org/journal/paperInfo/jnn?paperId=2195>
47. Zhi-Peng, S.; Lang, L.; Li, Z.; Dian-Zeng, J. Rapid synthesis of ZnO nano-rods by one-step, room-temperature, solid-state reaction and their gas-sensing properties. *Nanotechnology* **2006**, *17*, 2266–70. <https://dx.doi.org/10.1088/0957-4484/17/9/032>.
48. EL-Rafei, A.M.; Zawrah, M.F. Effect of alkali concentration and reaction time on the morphology of ZnO nano-microparticles prepared by hydrothermal method. *Journal of Ceramic Science & Technology* **2014**, *5*, 193–198, <https://doi.org/10.4416/JCST2014-00002>.
49. Moazzen, M.A.M.; Borghei, S.M.; Taleshi, F. Change in the morphology of ZnO nanoparticles upon changing the reactant concentration. *Applied Nanoscience* **2013**, *3*, 295–302, <https://doi.org/10.1007/s13204-012-0147-z>.
50. Wojnarowicz, J.; Opalinska, A.; Chudoba, T.; Gierlotka, S.; Mukhovskiy, R.; Pietrzykowska, E.; Sobczak, K.; Lojkowski, W. Effect of water content in ethylene glycol solvent on the size of ZnO nanoparticles prepared using microwave solvothermal synthesis. *Journal of Nanomaterials* **2016**, 1–15, <http://dx.doi.org/10.1155/2016/2789871>.
51. Jung, S.H.; Oh, E.; Lee, K.H.; Yang, Y.; Park, C.G.; Park, W.J.; Jeong, S-H. Sonochemical preparation of shape-selective ZnO nanostructures. *Crystal Growth & Design* **2008**, *8*, 265–269, <https://doi.org/10.1021/cg070296l>.
52. Lavand, A.B.; Malghe, Y.S. Synthesis, characterization and visible light photocatalytic activity of nitrogen-doped zinc oxide nanospheres. *Journal of Asian Ceramic Societies* **2015**, *3*, 305–310, <https://doi.org/10.1016/j.jascer.2015.06.002>.
53. Bian, S.W.; Mudunkotuwa, I.A.; Rupasinghe, T.; Grassian, V.H. Aggregation and dissolution of 4 nm ZnO nanoparticles in aqueous environments: influence of pH, ionic strength, size and adsorption of humic acid. *Langmuir* **2011**, *27*, 6059–6068, <https://doi.org/10.1021/la200570n>.

54. Pholnaka, C.; Sirisathitkula, C.; Suwanboon, S.; Harding, D.J. Effects of precursor concentration and reaction time on sonochemically synthesized ZnO nanoparticles. *Materials Research* **2014**, *17*, 405-411, <http://dx.doi.org/10.1590/S1516-14392013005000192>.

55. Long, T.F.; Yin, S.; Takabatake, K.; Zhang, P.; Sato, T. Synthesis and characterization of ZnO nanorods and nanodisks from zinc chloride aqueous solution. *Nanoscale Research Letters* **2009**, *4*, 247-253, <https://doi.org/10.1007/s11671-008-9233-2>.

56. Wu, H.B.; Chan, M.N.; Chan, C.K. FTIR characterization of polymorphic transformation of ammonium nitrate. *Aerosol Science & Technology* **2007**, *41*, 581-588, <https://doi.org/10.1080/02786820701272038>.

57. Max, J.J.; Chapados, C.J. Infrared Spectroscopy of Aqueous Carboxylic Acids: Comparison between Different Acids and Their Salts. *The Journal of Physical Chemistry: A* **2004**, *108*, 3324-3337, <https://doi.org/10.1021/jp036401t>.

58. Imran, K.; Khan, S.; Nongjai, R.; Ahmed, H.; Khan, W. Structural and optical properties of gel-combustion synthesized

Zr doped ZnO nanoparticles. *Optical Materials* **2013**, *35*, 1189-1193, <https://doi.org/10.1016/j.optmat.2013.01.019>.

59. Yung, M.M.N.; Mouneyrac, C.; Leung, K.M.Y. Ecotoxicity of zinc oxide nanoparticles in the marine environment. *Encyclopedia of Nanotechnology* **2014**, 1-17, [https://doi.org/10.1007/978-94-007-6178-0\\_100970-1](https://doi.org/10.1007/978-94-007-6178-0_100970-1)

60. Harding, F. *Breast Cancer: Cause – Prevention – Cure*. Tekline Publishing, 2006.

61. Hasnidawani, J.N.; Azlina, H.N.; Norita, H.; Bonnia, N.N.; Ratim, S.; Ali, E.S. Synthesis of ZnO nanostructures using sol-gel method. *Procedia Chemistry* **2016**, *19*, 211-216, <https://doi.org/10.1016/j.proche.2016.03.095>.

62. Brintha, S.R.; Ajitha, M. Synthesis and characterization of ZnO nanoparticles via aqueous solution, sol-gel and hydrothermal methods. *IOSR Journal of Applied Chemistry* **2015**, *8*, 66-72, <https://doi.org/10.9790/5736-081116672>

63. Ghasemzadeh, M.A.; Safaei-Ghomi, J. Synthesis and characterization of ZnO nanoparticles: Application to one-pot synthesis of benzo[b][1,5]diazepines *Cogent Chemistry* **2015**, *1*, <https://doi.org/10.1080/23312009.2015.1095060>.

## 6. ACKNOWLEDGEMENTS

The authors acknowledge the contribution of colleagues from Faculty of Resource Science and Technology (FRST), Geochemistry Laboratory and Analytical Laboratory, Universiti Malaysia Sarawak. This research was supported by Universiti Malaysia Sarawak, Tun Openg Chair, with Research Grant Code: F07/TOC/1738/2018.



© 2020 by the authors. This article is an open access article distributed under the terms and conditions of the Creative Commons Attribution (CC BY) license (<http://creativecommons.org/licenses/by/4.0/>).